Emittance measurements and minimization at the SwissFEL Injector Test Facility

Eduard Prat,* Masamitsu Aiba, Simona Bettoni, Bolko Beutner,†
Sven Reiche, and Thomas Schietinger
Paul Scherrer Institut, CH-5232 Villigen PSI, Switzerland
(Received 24 July 2014; published 13 October 2014)

The emittance of the electron beam is crucial for Free-Electron Laser facilities: it has a strong influence on the lasing performance and on the total length of the accelerator. We present our procedure to measure and minimize the projected and slice emittance at the SwissFEL Injector Test Facility. The normalized slice emittance resolution achieved is about 3 nm and the longitudinal resolution is about 13 fs, with measurement errors estimated to be below 5%. After performing a full optimization we have obtained, for uncompressed beams, a slice emittance of about 200 nm for a beam charge of 200 pC, and a slice emittance of about 100 nm for 10 pC. These values are consistent with our simulations and are well below the requirements of the SwissFEL under construction at the Paul Scherrer Institute. At these bunch charges our measured slice emittances are, to our knowledge, the lowest reported so far for an electron linear accelerator.

DOI: 10.1103/PhysRevSTAB.17.104401 PACS numbers: 29.20.Ej, 41.60.Cr, 41.85.-p, 29.27.Fh

I. INTRODUCTION

The SwissFEL facility under construction at the Paul Scherrer Institute will produce coherent, bright, and short photon pulses covering a wavelength range down to 1 Å. This requires normalized emittances below 0.18 μm and 0.43 μm for bunch charges between 10 pC and 200 pC, respectively [1]. To demonstrate the feasibility of our beam design the SwissFEL Injector Test Facility was built and has been operated since 2010 [2].

The electron beam emittance is of great importance for Free-Electron Laser (FEL) facilities. First, transversely coherent FEL radiation is generated if $\varepsilon_n/\gamma \approx \lambda/4\pi$, where ε_n is the normalized beam emittance, γ is the Lorentz factor and λ is the FEL radiation wavelength. This condition entails that by reducing the normalized emittance the final beam energy can be decreased, which translates into a more compact and affordable accelerator. Second, a smaller emittance implies a higher radiation power and a shorter undulator beamline to reach FEL saturation. To illustrate the effect of the emittance on the final FEL performance, Fig. 1 shows the dependence of the FEL power on the emittance for the 200 pC charge operation mode of SwissFEL.

The natural length scale along the bunch to analyze beam properties related to the FEL performance is the slippage length, defined as the longitudinal slippage of the electrons with respect to the photons over the undulator length. The slippage length typically corresponds to a small fraction of the electron bunch. In the SwissFEL case, for a wavelength of 1 Å at 200 pC the rms bunch length is about 6 μm and the slippage length is about 0.3 μm. Thus longitudinally resolved emittance studies, so-called slice emittance measurements, are of great significance at FEL facilities.

The emittance of the whole bunch, the so-called projected emittance, is a general indicator of the electron beam

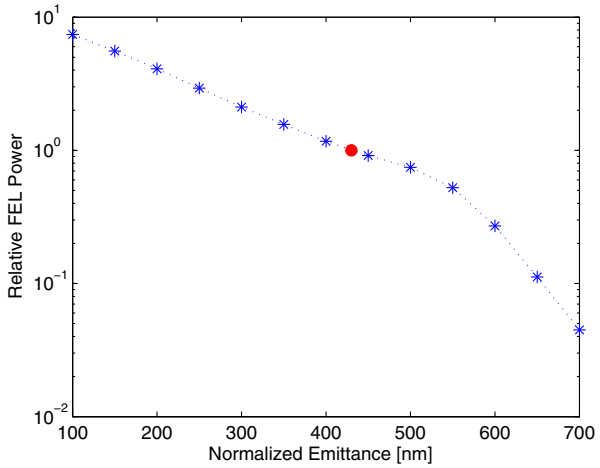

FIG. 1. Relative FEL power as a function of the normalized emittance. The reference case (100% relative FEL power) corresponding to the nominal emittance of 0.43 μm is indicated by a red dot. The calculations are done with *Genesis* [3] after 12 undulator modules for the SwissFEL design parameters at 200 pC [1]. We note that the FEL process does not reach saturation within 12 modules for normalized emittances larger than 550 nm.

*eduard.prat@psi.ch
†Present address: Deutsches Elektronen-Synchrotron, Notkestrasse 85, D-22607 Hamburg, Germany.

quality. Centroid-offset or beam-size variation along the bunch, which may not affect the slice emittance, but cause an increase of the projected emittance, can deteriorate the FEL performance. Therefore, both slice and projected emittance need to be measured and minimized. Extensive worldwide research and development have been performed in the last years to reduce the emittance of FEL drive beams, see for example Refs. [4–6].

To achieve the possible minimum emittance at a given machine, it is important to establish a reliable measurement method. A high resolution in the measurement is quite useful during the minimization because, for example, it facilitates finding the minimum emittance value and corresponding machine setting from an emittance measurement as a function of machine parameter(s). In addition, small emittance values cannot be confirmed if the resolution is poor. We present here our methods to measure and minimize the emittance for uncompressed beams at the SwissFEL Injector Test Facility, which achieved slice emittances of about 200 nm for 200 pC and of about 100 nm for 10 pC. This includes our experience using a recent development of a high-resolution beam screen [7].

After an introduction to the SwissFEL Injector Test Facility (Sec. II) we describe in Sec. III the methods used for our transverse phase-space measurements. The emittance minimization techniques applied and the results obtained are presented in Sec. IV.

II. THE SWISSFEL INJECTOR TEST FACILITY

Figure 2 shows a sketch of the SwissFEL Injector Test Facility. Electron bunches of charges between 10 pC and 200 pC are generated in a 2.6-cell standing-wave S-band RF photo-injector gun, originally developed for high-current operation at the CLIC test facility (CTF2) at CERN [8]. A copper photo-cathode is employed. The gun drive laser is based on a Ti:Sapphire chirped pulse amplification system [9]. A longitudinal flat-top profile is approximated by pulse stacking of 32 replicas. The FWHM pulse lengths are 9.9 ps and 3.7 ps for charges of 200 pC and 10 pC, respectively. The total electron energy at the gun exit is 7.1 MeV. A solenoid close to the gun cavity is used for initial focusing (invariant envelope matching [10]). Additional individually powered windings inside the gun solenoid allow for correction of normal- and skew-quadrupole field components.

Four S-band accelerating structures bring the beam energy up to the nominal value of 250 MeV. For the measurements presented here the structures are operated on-crest to maximize the energy gain. The last two structures may be operated off-crest to generate the required energy chirp to longitudinally compress the beam. Additional solenoid magnets around these structures allow for further control of the transverse optics. After some space, where an X-band linearizing system and a bunch-compressor chicane are placed, an S-band transverse deflecting cavity is used for longitudinally resolved measurements such as bunch length and slice emittance. A dedicated beam diagnostic section downstream of the deflecting cavity allows us to characterize the accelerated beam. Several quadrupole magnets and beam screens measuring the transverse beam profile are available for the emittance measurement. The final beam energy is measured by a spectrometer at the end of the diagnostic section.

More details on the SwissFEL Injector Test Facility can be found in Ref. [2].

III. EMITTANCE MEASUREMENT PROCEDURE

The moments of phase-space distributions can be determined by varying the betatronic beam transport between a reference point and a transverse beam profile monitor used for beam size measurements. Specifically, considering the horizontal plane, we obtain the beam moments $\langle x_0^2\rangle$, $\langle x_0'^2\rangle$, and $\langle x_0 x_0'\rangle$ at the reference point from N measured beam sizes σ_i by using the corresponding transport matrices R^i and solving the system of equations

$$\sigma_i^2 = {R_{11}^i}^2\langle x_0^2\rangle + {R_{12}^i}^2\langle x_0'^2\rangle + 2R_{11}^i R_{12}^i\langle x_0 x_0'\rangle, \quad (1)$$

for $i = 1, \ldots, N$. From the measured beam moments the emittance and Twiss parameters can be derived as

$$\varepsilon_x = \sqrt{\langle x_0^2\rangle\langle x_0'^2\rangle - \langle x_0 x_0'\rangle^2}, \quad (2)$$

$$\alpha_x = -\langle x_0 x_0'\rangle/\varepsilon_x, \qquad \beta_x = \langle x_0^2\rangle/\varepsilon_x, \qquad \gamma_x = \langle x_0'^2\rangle/\varepsilon_x. \quad (3)$$

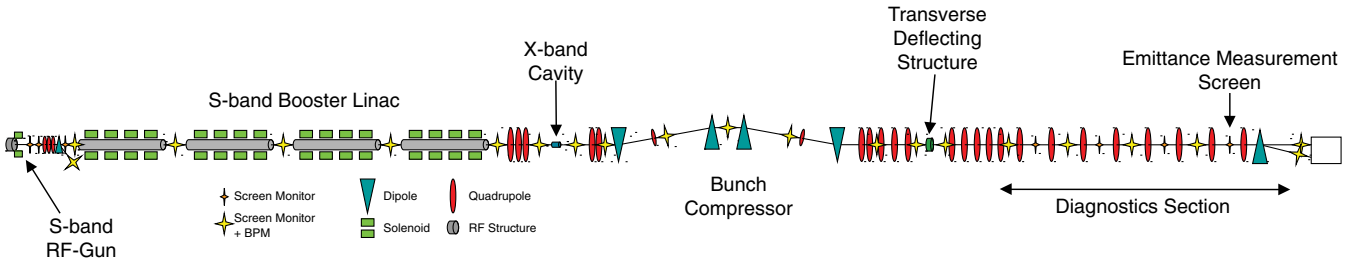

FIG. 2. Schematic layout of the SwissFEL Injector Test Facility (not to scale). The total length is about 60 m.

The normalized emittance is obtained by multiplying the emittance by the relativistic $\beta\gamma$:

$$\varepsilon_{n,x} = \frac{p}{mc}\varepsilon_x, \tag{4}$$

where p is the central momentum of the beam, m is the particle rest mass and c is the speed of light.

Although a set of three beam size measurements for different transport functions is sufficient to obtain the emittance and Twiss parameters, we use a much larger number of measurements and solve Eq. (1) by a least-square fitting, thereby increasing the robustness against measurement errors. A detailed description of this procedure can be found, e.g., in Ref. [11].

In the above procedure we have referred only to the horizontal plane, but the same treatment is valid for the vertical phase-space (y, y').

Our procedure is generic in the sense that it can also be used for slice emittance measurements in combination with a transverse deflecting cavity, as illustrated in Fig. 3. Such a structure induces a time-dependent transverse kick onto the bunch. It results in a transverse streak of the beam at a downstream measurement location. The beam size in the streaking plane, which is the vertical plane at the SwissFEL Injector Test Facility, is proportional to the bunch length.

To find the coefficient relating the observed beam size to the bunch length we use a direct calibration where we measure the vertical centroid position on the screen for various cavity phases. Since the cavity frequency is known, the coefficient can easily be found from such a measurement. Furthermore, this calibration measurement can be performed expeditiously and the coefficient can be updated for each measurement.

The local beam size along the bunch, in the direction perpendicular to the streak, can be found by "slicing" the streaked beam image. Finally, the slice emittances are computed as described above. We note that the least-square fitting is applied individually for each slice.

A. Measurement optics and beam matching

A set of transport matrices R^i is required for the emittance measurement, as discussed above. A simple measurement using one single quadrupole to vary R^i is widely applied. One normally needs two measurements, one for the horizontal plane and the other for the vertical plane, such that the beam size measurement as a function of quadrupole strength covers the minimum beam size of the plane under measurement. In other words, the phase advance between the scanning quadrupole and the measurement location needs to be varied, ideally covering the range from 0° to 180°.

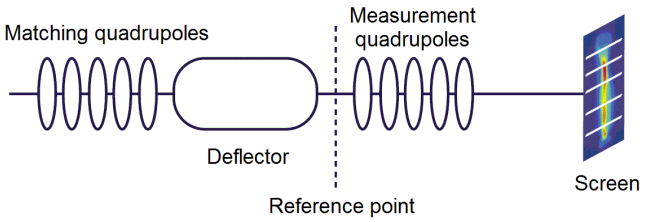

FIG. 3. Schematic overview of the setup for slice emittance measurements at the SwissFEL Injector Test Facility.

For a reliable measurement a careful setup of the measurement configuration and the incoming beam optics (Twiss parameters) is needed. When the distance between the quadrupole and the beam size monitor is too short and/or the β-function at the quadrupole is too large, the minimum beam size may become so small that the measurement is compromised by the monitor resolution. We therefore first define a measurement optics at the reference point (see Fig. 3) upstream of the scanning quadrupole such that the beam size at the monitor is much larger than its resolution limit. Second, the measurement is repeated to update the matching quadrupole strengths until the incoming beam optics are matched to the measurement optics. The matching quadrupoles are situated upstream of the reference point.

We employ an advanced method to measure the projected emittance, a symmetric single quadrupole scan [12], where the measurement optics at the quadrupole are chosen to ensure minimum beam size in both planes for zero quadrupole gradient. One of the advantages of the method is that only one measurement is required to determine the horizontal and vertical emittances simultaneously.

The slice emittance measurement requires more control over the measurement optics. The set of optics transfer matrices should respect certain boundary conditions: the phase advance between the deflector and the screen in the measurement plane (horizontal plane in our case) should cover as much of the 180° range as possible, while in the streak direction (the vertical plane in our case) a constant phase advance fulfilling $\sin\mu_y = 1$ optimizes the resolution of the deflector. The β-function in the streak direction at the deflecting cavity needs to be large for an efficient streaking. The β-function in the measurement plane should be large at the beam size monitor to optimize the resolution.

This level of optics control cannot be achieved by a single quadrupole; we therefore use multiple quadrupoles. Emittance measurements using multiple quadrupoles were originally studied in Ref. [13]. The optics setup used for our slice emittance measurements is illustrated in Fig. 4. The β-function in the horizontal plane varies between 35 m and 40 m for the whole scan to obtain beam sizes that can be measured conveniently for typical emittance values. The β-function in the vertical direction is kept below 10 m to fit the streaked beam to the beam screen. Again, the precalculated k-values, as shown in the bottom plot of Fig. 4 for the slice measurement, will result in the desired measurement optics only if the incoming beam optics are matched to the measurement optics at the reference point.

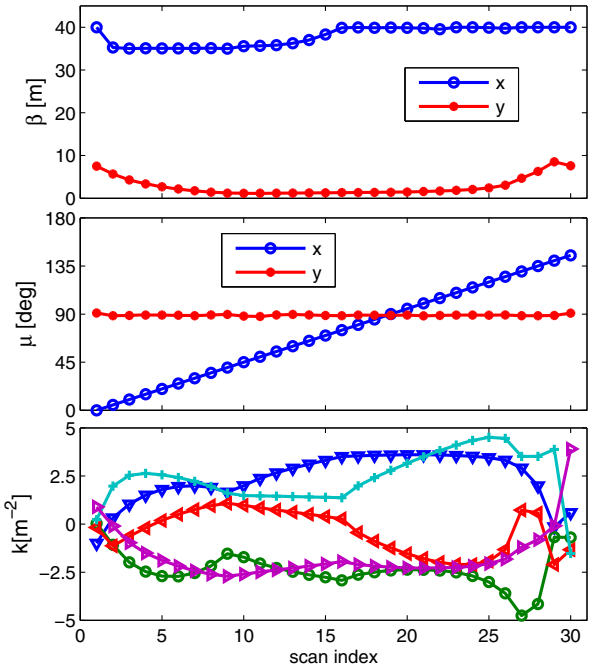

FIG. 4. Optics for the slice emittance measurements. The β-functions at the measurement screen (top), phase advance between deflector and screen (middle), and the required k-values for the measurement quadrupoles during the scan (bottom), plotted for each scan index i.

Our strategy therefore is to match the incoming beam optics based on the projected emittance measurement first, followed by the slice emittance measurement. The beam optics may, however, vary along the bunch such that the projected beam optics differ from the optics at the longitudinal core of the bunch, thereby distorting the measurement. The longitudinally resolved beam-size measurements allow us to match the (horizontal) optics of an arbitrary slice of the bunch to the measurement optics. The core slice, defined as the slice with highest local current, is usually selected for the matching, since it is the most relevant slice for the lasing process.

As a typical example, Fig. 5 shows a comparison of matching iterations of the core slice optics. Similar to the matching of the projected bunch, we examine the reconstructed Twiss parameters of the beam core slice and compute corrections for a set of upstream matching quadrupoles to match the beam core to the measurement optics. Since the measurements can be compromised by the initial mismatch several iterations may be needed as illustrated in Fig. 5. As a general rule we consider measurements only to be reasonable if the local mismatch parameter, defined as $\xi = (\beta_0\gamma - 2\alpha_0\alpha + \gamma_0\beta)/2$ (the subscript 0 denotes the design values) [14] is close to unity. Typically we repeat both the initial projected matching iterations and the core slice matching until mismatch parameters below 1.1 are reached, before we trust our measured emittance values.

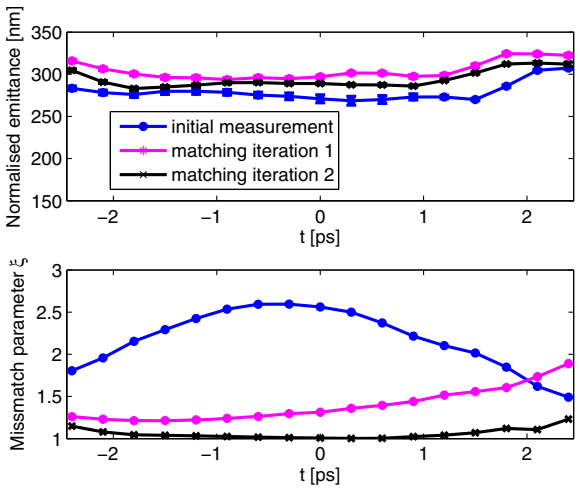

FIG. 5. An example of matching iterations of the longitudinal beam core. The emittance measurements (top) are compared with the mismatch parameter ξ along the bunch (bottom). The beam charge is 200 pC.

B. Beam size determination

The quality of the beam-size measurements is critical for the emittance determination. Our primary transverse profile monitor consists of a scintillating screen made of yttrium-aluminum-garnet (YAG) crystal. The screen setup is optimized for resolution through a proper choice of the observation angle, which mitigates effects arising from crystal thickness [7] (the scintillator is placed at an angle of 8.1 degrees with respect to the electron beam and has a thickness of 100 μm).

The transverse beam sizes in the projected emittance measurement are determined by fitting Gauss functions to the projections of the background-subtracted beam images. To obtain the longitudinally resolved horizontal beam sizes we divide the beam image into appropriate bands, corresponding to slices of the bunch.

Particular attention must be given to the requirement that a set of beam-size measurements σ_i for a given scan index i refer to the same physical longitudinal slice along the bunch, as shot-to-shot variations of beam arrival time, deflector RF phase or beam position may affect the actual position of slices on the screen. This is ensured by identifying a reference point in each image and mapping the slices with respect to this reference. In practice we determine the longitudinal centroid position of the bunch individually for each image by means of a Gauss fit. This is possible since in our case the bunches typically have a smooth and approximately symmetric longitudinal profile. The transverse beam sizes σ_i of the slices are also determined from Gauss fits to the horizontal profiles within the respective slices. An example is shown in Fig. 6. We note that no charge cut is applied to the beam images for the determination of the beam sizes, i.e., the Gauss fits are applied to the full data set.

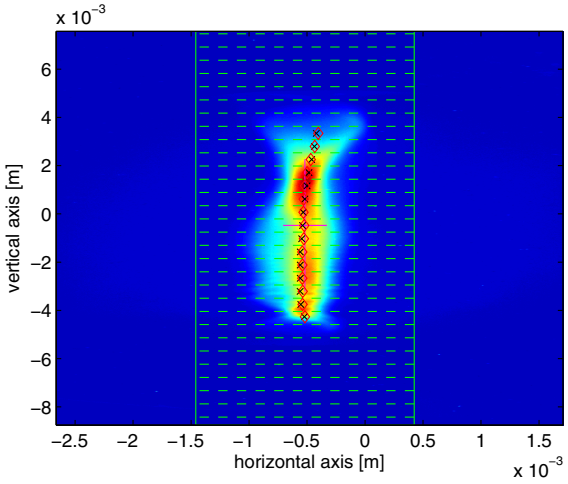

FIG. 6. Typical image of the deflected beam at the transverse profile monitor. The streak correlates the vertical with the longitudinal direction, and the slice emittance is reconstructed in the horizontal plane. Around the centroid (magenta cross) a region-of-interest is defined (green box), which is further divided into slices (dashed green lines). Centroid positions within each slice are calculated (red diamonds) and compared with the center of a Gaussian fit (black crosses).

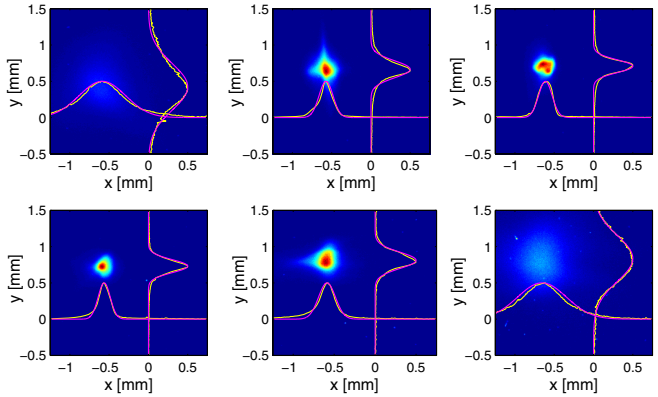

FIG. 7. Six out of the sixteen transverse beam images of a projected emittance measurement at 200 pC. The horizontal and vertical phase advances between each of the distributions are 30 degrees. The yellow lines are the projections to the horizontal and vertical axes and the magenta lines correspond to the Gaussian fits.

After extensive work on image analysis (see Refs. [15–17]), we have come to the conclusion that in principle the rms method, applied in conjunction with a suitably tuned noise subtraction algorithm, results in a more accurate measurement of the statistical emittance for the most general class of beam profiles. In practice, however, for the case of our beam profiles after optimization, the application of Gauss fits turns out to be significantly faster and more robust while giving essentially equivalent results. In our context of FEL development the use of Gauss fits is furthermore justified by the fact that only the core part of the beam profile will contribute to the lasing process. The second moments of this core part are well characterized by Gauss fits, as illustrated in Fig. 7, which shows a few examples from a projected emittance measurement at 200 pC.

C. Measurement resolution and errors

The emittance resolution is the square of the beam-size resolution divided by the β-function at the profile monitor. We have determined the spot size resolution experimentally by strongly focusing the beam onto the screen. From these measurements we estimate the beam-size resolution to be 15 μm or better. This corresponds, for a beam energy of 250 MeV, to a normalized slice emittance resolution of about 3 nm and to a normalized projected emittance resolution of about 4 nm. This is achieved with our relatively large β-functions at the measurement location (between 35 m and 40 m for the slice emittance measurement, see Fig. 4). The photon yield from the YAG crystal gives a good signal-to-noise ratio for bunch charges of 1 pC and less: the signal-to-noise ratio of the system (maximum signal divided by rms noise) is 20000 or better, while for a typical measurement with a beam charge of 1 pC the signal-to-noise is still around 100.

The longitudinal resolution is determined by the streak voltage and the transfer matrix element R_{34} between the deflector and the screen. With the phase advance adjusted to $\sin\mu_y \approx 1$, and a value of the vertical β-function of 40 m at the deflector we obtain a longitudinal resolution of about 13 fs. This resolution is reached for the maximum voltage of 5 MV in the deflecting structure, and assuming a normalized vertical emittance $\varepsilon_{n,y}$ of 500 nm for a beam energy of 250 MeV.

The statistical errors on the measured emittance reported here are obtained by propagating statistical beam-size errors according to Eq. (1). For example a 5% beam-size measurement error results in about 2.7% emittance error (slice or projected) if the phase advance $\Delta\mu$ per step i is 10°.

The systematic errors are of the same order of magnitude as the statistical ones. Contributions from the camera pixel size calibration and the imaging optics resolution are estimated to be on the order of 1% to 2%. Since the beam sizes are determined by Gauss fits, any deviation of the beam profile from a Gaussian shape can result in a systematic error. For our almost Gaussian beam profiles this effect is small and again estimated to be at the percent level.

Beam-energy and quadrupole-field errors modify the R^i transfer functions, leading to differences between the real beam transport and the fit to Eq. (1). Moreover, an energy uncertainty also contributes to the error of the normalized emittances. At the SwissFEL Injector Test Facility, the quadrupole field error is about 0.2% and the energy error is about 0.1%, which translates into an error on the derived emittances of well below 0.5%. As described above we

match the beam to the design optics such that possible error contributions from an optics mismatch are minimized. The remaining contribution to the error is estimated to be below 1%. The fact that the matching iterations converge quickly, as shown in Fig. 5, gives us additional confidence in our results. Any significant error in the determination of beam moments would result in a much worse convergence behavior, and we would not consistently attain a mismatch of $\xi = 1$ for the beam core—unless there is a global scaling error.

IV. EMITTANCE MINIMIZATION AND RESULTS

The emittance at the source is determined by three different contributions related to thermal emittance, space charge, and the RF field, respectively. We have optimized the injector parameters with numerical simulations using Astra [18] and an optimizer [19]. The latter generates input files, runs the simulations and uses the outputs to minimize the figure of merit, defined as a weighted average of the slice emittance and the mismatch parameter between the slices in the central part of the bunch. The figure of merit is $\epsilon_n[\mu\mathrm{m}] + 0.1\xi$—in this way both magnitudes have approximately the same weight. The gun gradient is set to the maximum possible compatible with the technology of the RF gun. The maximum field along the longitudinal axis of 100 MV/m corresponds to an energy at the exit of the gun of 7.1 MeV. The laser spot size and the field generated by the gun solenoid are determined by the optimizer to counteract the contributions of the thermal emittance (smaller for smaller spot size) and space charge (smaller for larger spot size) to the final emittance. For the optimizations we assume a normalized thermal emittance of 600 nm/mm, as expected based on the measurements reported in Ref. [20]. For the 200 pC case we obtain a normalized slice emittance in the central part of the bunch and a projected emittance of 194 ± 19 nm (the error indicates the standard deviation of the slices) and 250 nm, respectively (see Table II). For the 10 pC case we rescale the laser size to have a constant three-dimensional charge density and fix the pulse length according to the peak current at the end of the injector. For this case the normalized slice emittance is 56 ± 1 nm and the projected emittance is 60 nm. The optimum rms laser beam sizes for the 200 pC and 10 pC cases are about 0.20 mm and 0.07 mm, respectively.

In the measurements the performance of the laser system, in particular the transverse size and homogeneity of the laser spot on the cathode, are essential for reaching low emittance. We set the laser aperture to have an rms laser beam size at the cathode as close as possible to the optimum values obtained in our simulations: 0.23 mm for the 200 pC case and 0.12 mm for the 10 pC configuration.

On the accelerator side the setup of the gun RF cavity is essential. The effective energy gain as well as the relative phase between laser arrival time and gun RF need to be tuned while observing the beam in a dipole spectrometer: the gun phase is set to minimize the energy spread, i.e., the beam size in the spectrometer profile monitor.

After the setup of the longitudinal dynamics in the gun we adjust the gun main solenoid focusing to the beam charge and energy so as to minimize the resulting emittance. Residual quadrupole components in the gun solenoid are compensated by skew and normal quadrupole correctors integrated into the main solenoid. One objective of this initial beam tuning is the observation of a transverse beam image of azimuthal symmetry at a screen upstream of the first symmetry-breaking quadrupole.

For more details on the beam dynamics in the electron gun we refer to [2].

For uncompressed beams (our measurements presented here) emittance degrading effects in the downstream beamline are dominated by off-axis RF fields and wake fields due to misalignments in the S-band booster structures or incoming trajectory errors. (In the case of compressed beams additional effects arise from coherent synchrotron radiation and longitudinal space charge.) An effective handle to suppress emittance degradation in the S-band booster is the beam orbit: since the structures are physically fixed, reference centers of the beam position monitors are shifted so as to minimize the orbit change induced by a variation of RF voltage, thus defining an optimum orbit. We then employ an orbit feedback to maintain the optimum orbit during our emittance measurements.

Coupling between the x- and y-planes increases the apparent emittance, unless the intrinsic emittance in an appropriately rotated coordinate system is measured. Moreover the FEL performance is deteriorated when the coupling is significant. For the projected emittance measurement, the intrinsic emittances can be computed by measuring the x-y correlation in addition to the horizontal and vertical beam sizes. This is not possible for the slice emittance measurement. We therefore correct the linear coupling of the projected beam using available knobs.

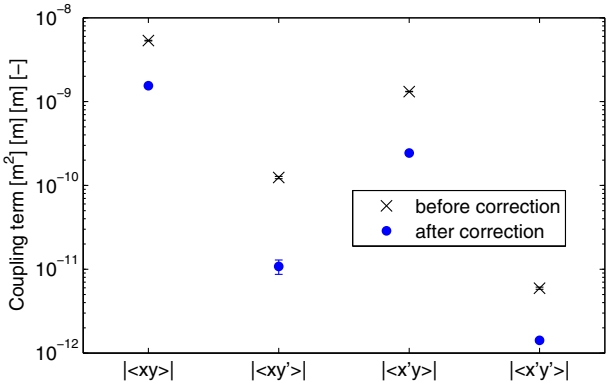

FIG. 8. Coupling correlations before and after the correction. The coupling contribution to the emittance was reduced from 11.3% to 0.6%.

TABLE I. A summary of "knobs" used for emittance minimization.

Knob	Physics effect	Comment
Laser spot size on cathode	Invariant envelope matching	Iris set according to simulated optimum
Transverse laser profile	Emittance x-y symmetry	Tuned to maximum homogeneity and symmetry
Longitudinal laser profile	Collective effects in the gun	Tuned to flat top (lower emittance)
Laser alignment	Orbit, dispersion	Standard beam-based alignment
Gun phase	Minimization of energy spread	Minimization of horizontal beam size in spectrometer
Gun gradient	Invariant envelope matching	Set to design energy using spectrometer (7.1 MeV)
Gun solenoid alignment	Orbit, dispersion	Standard beam-based alignment
Gun solenoid field	Invariant envelope matching	Emittance-based optimization
Corrector quads	x/y coupling	Empirical and systematic tuning
S-band solenoid fields	Invariant envelope matching, x-y coupling	Empirical and systematic tuning
Orbit in S-band booster	Wake- and off-axis RF fields	Emittance-driven beam-based alignment
Orbit after S-band booster	Dispersion at screen	Beam-based alignment and local orbit bump

The goal is to minimize the coupling contribution to the emittance. Our approach consists in measuring and correcting the coupling terms with the gun corrector quadrupoles and four solenoids around the booster accelerating structures. These knobs are varied in turn and the coupling correlations are measured. The result is a sensitivity matrix, which relates an excitation of the correction knobs to the corresponding change in the coupling correlations. A matrix inversion is applied to find an optimum setting of the correction knobs. In this way the linear coupling was corrected down to a negligible level, as shown in Fig. 8. A full description of the coupling measurement and correction procedure can be found in [21].

A further source of degradation is the spurious dispersion. We have to ensure that dispersion does not affect the beam-size measurement at the screen location. Our emittance measurement based on Eq. (1) does not include dispersion effects. The spurious dispersion varies during the measurement since the quadrupole strengths are changing. It is not straightforward to measure all $R^i_{n,6}(n = 1, 2, 3, 4)$ elements between the reference point and the measurement screen. A beam-based alignment was applied to minimize the spurious dispersion but it is valid for a fixed quadrupole setting only. A simple but effective mitigation strategy is to generate local orbit bumps at the screen until the observed emittance is minimized. This compensates at least the average effect of the dispersion terms. For compressed beams with a larger energy spread (energy chirp), a more sophisticated approach may be necessary.

A summary of the various optimization techniques is given in Table I.

The results of our emittance optimization for the SwissFEL standard operation modes are summarized in Table II. The slice emittance measurements are shown graphically in Figs. 9 and 10 for 10 pC and 200 pC bunch charge, respectively. We achieved core slice emittances of $\varepsilon_x = 98 \pm 2$ nm rad for the 10 pC mode and $\varepsilon_x = 199 \pm 15$ nm rad for the 200 pC mode. These values are obtained by averaging the emittance over five slices around the beam core. The error bars consider the variation of the emittance along the slices and the statistical uncertainties of the emittance measurement. There is a good agreement between the measured and the simulated results for a beam charge of 200 pC. For the 10 pC case the agreement is reasonable but not quite as good. This is because the laser spot size for those measurements (about 0.12 mm) was significantly larger than the simulated optimum (about

TABLE II. Measured and simulated core slice and projected emittances for different bunch charges. Measurement errors are statistical (see text for details).

	Measurements			Simulations	
Q [pC]	$\varepsilon^{\text{slice}}_{n,x}$ [nm]	$\varepsilon^{\text{proj}}_{n,x}$ [nm]	$\varepsilon^{\text{proj}}_{n,y}$ [nm]	$\varepsilon^{\text{slice}}_{n}$ [nm]	$\varepsilon^{\text{proj}}_{n}$ [nm]
≈200	199 ± 15	280 ± 3	324 ± 4	194 ± 19	250
≈10	98 ± 2	116 ± 1	162 ± 1	56 ± 1	60
≈0.03	24.2 ± 0.9	33.0 ± 0.2	29.3 ± 0.5	⋯	⋯

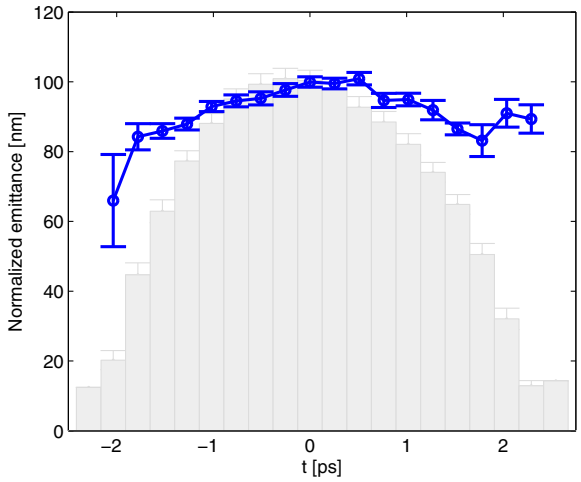

FIG. 9. Normalized slice emittance in the horizontal plane for a bunch charge of 10 pC (blue). The error bars are obtained by error propagation of the statistical beam-size errors. The longitudinal bunch charge profile is shown in gray bars.

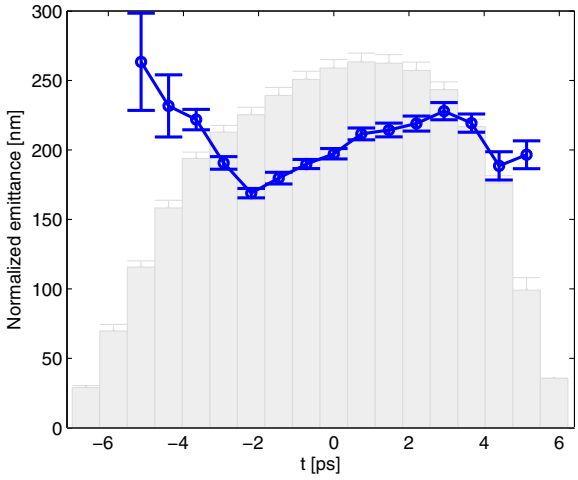

FIG. 10. Same as Fig. 9 for a bunch charge of 200 pC.

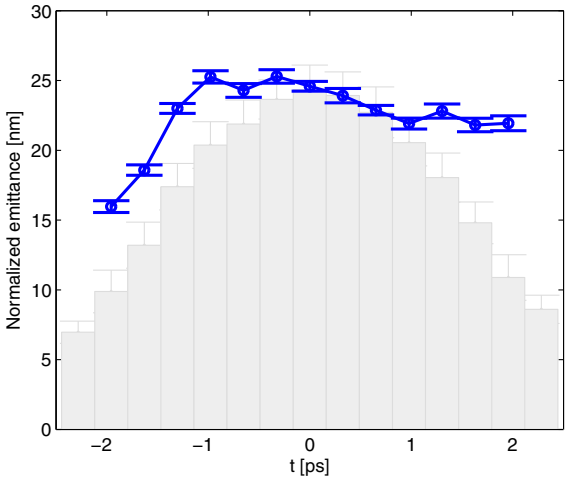

FIG. 12. Same as Fig. 9 for a bunch charge of about 30 fC.

0.07 mm). It was not possible, due to the limited range of available laser apertures, to set the laser size to 0.07 mm. We note that for SwissFEL we will have a continuous aperture to confine the laser spot to any required size. In any case, for both the 200 and 10 pC cases the obtained emittances are below the tight requirements of SwissFEL.

Figure 11 shows a typical longitudinal laser profile for a bunch charge of 200 pC and the transverse laser distribution at the cathode for the measurements done at 200 pC. Equivalent laser distributions are obtained for a beam charge of 10 pC.

Our measured emittances are stable in the short term, i.e., the reconstructed emittances from consecutive measurements have shown no significant differences. As long as the laser beam quality remains the same, we are able to reproduce the slice emittance values presented here with very similar machine settings.

The excellent performance of our transverse profile monitor setup allows us to study bunch charges lower than 10 pC, which is the minimum design charge for SwissFEL operation. We were able to resolve slice emittance in bunches with charge down to about 30 fC. The observed slice emittance for this charge was $\varepsilon_x = 24.6 \pm 0.4$ nm rad (see Fig. 12). The rms laser spot size on the cathode was about 50 μm in this case. Although such a low-charge beam is not foreseen for SwissFEL, this measurement corroborates our confidence in the emittance measurement procedure, which we apply to the wide range of SwissFEL bunch charges from 10 pC to 200 pC.

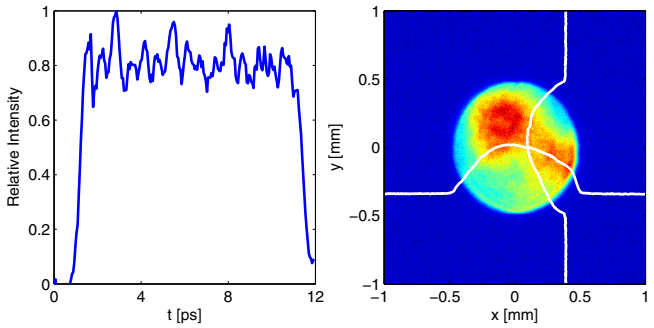

FIG. 11. Left: typical temporal laser profile for a bunch charge of 200 pC. Right: spatial laser profile at the cathode for the measurements done at 200 pC (the white lines are the projections onto the horizontal and vertical axes).

V. CONCLUSIONS

The transverse beam emittance is one of the most important parameters for FELs. We have established a precise method of high-resolution to measure the emittance: the measurement error is below the 5% level, the normalized emittance resolution is about 3 nm, and the longitudinal resolution is about 13 fs.

Measurements carried out at the SwissFEL Injector Test Facility with uncompressed beams have demonstrated emittances well suitable for SwissFEL operation and consistent with simulations. After a full optimization of the electron beam we could achieve slice emittances of about 200 nm for 200 pC and about 100 nm for 10 pC. These are, to our knowledge, the lowest slice emittances ever realized and measured in a linear accelerator. We emphasize that establishing a reliable measurement procedure with high resolution is crucial to optimize the emittance toward very low values.

Current efforts at the test facility are focused on emittance studies with compressed beams, using a magnetic compression chicane in combination with an X-band phase-space linearizing system, and will be presented in a future publication.

ACKNOWLEDGMENTS

The profile monitor used in our measurements at the SwissFEL Injector Test Facility was developed and

implemented by Rasmus Ischebeck. We would like to thank Hans Braun and Terry Garvey for fruitful discussions and careful proofreading of the manuscript. We acknowledge the extensive contributions of all PSI expert groups and the SwissFEL team to the construction and operation of the SwissFEL Injector Test Facility.

[1] R. Ganter, PSI Report No. 10-04, 2012.
[2] M. Pedrozzi, PSI Report No. 10-05, 2010.
[3] S. Reiche, Nucl. Instrum. Methods Phys. Res., Sect. A **429**, 243 (1999).
[4] D. H. Dowell, P. R. Bolton, J. E. Clendenin, P. Emma, S. M. Gierman, W. S. Graves, C. G. Limborg, B. F. Murphy, and J. F. Schmerge, Nucl. Instrum. Methods Phys. Res., Sect. A **507**, 327 (2003).
[5] F. Zhou, A. Brachmann, P. Emma, S. Gilevich, and Z. Huang, Phys. Rev. ST Accel. Beams **15**, 090701 (2012).
[6] M. Krasilnikov *et al.*, Phys. Rev. ST Accel. Beams **15**, 100701 (2012).
[7] R. Ischebeck and E. Prat (to be published).
[8] R. Bossart and M. Dehler, in *Proceedings of the 5th European Particle Accelerator Conference, Sitges, Spain, 1996* (IOP, Bristol, 1996), p. 1544.
[9] A. Trisorio, P. M. Paul, F. Ple, C. Ruchert, C. Vicario, and C. P. Hauri, Opt. Express **19**, 20128 (2011).
[10] L. Serafini and J. B. Rosenzweig, Phys. Rev. E **55**, 7565 (1997).
[11] F. Löhl, Master's thesis, University of Hamburg, 2005.
[12] E. Prat, Nucl. Instrum. Methods Phys. Res., Sect. A **743**, 103 (2014).
[13] P. G. Tenenbaum, Emittance Measurements in CTF 2 Drive Beam, CLIC-Note No. 326, 1997.
[14] M. Minty and F. Zimmermann, *Measurement and Control of Charged Particle Beams* (Springer, Berlin, 2003).
[15] B. Beutner and E. Prat, in *Proceedings of the 33rd International Free-Electron Laser Conference, Shanghai, China, 2011* (SINAP, Shanghai, 2012), p. 231.
[16] B Beutner, R. Ischebeck, and T. Schietinger, in *Proceedings of the 25th Linear Accelerator Conference, Tsukuba, Japan, 2010* (Jacow, Geneva, 2011), p. 653.
[17] B. Beutner, in *Proceedings of the 31st International Free-Electron Laser Conference, Liverpool, United Kingdom, 2009* (Jacow, Geneva, 2010), p. 111.
[18] K. Floettmann, ASTRA User's Manual, 2000, http://www.desy.de/~mpyflo/Astra_dokumentation/.
[19] S. Bettoni, M. Pedrozzi, and S. Reiche, in *Proceedings of the 35th International Free-Electron Laser Conference, New York, USA, 2013* (JACoW, Geneva, 2013), p. 219.
[20] E. Prat, S. Bettoni, H. H. Braun, M. C. Divall, R. Ganter, C. P. Hauri, T. Schietinger, A. Trisorio, and C. Vicario, in *Proceedings of the 36th International Free-Electron Laser Conference, Basel, Switzerland, 2014*, THC02 (to be published).
[21] E. Prat and M. Aiba, Phys. Rev. ST Accel. Beams **17**, 052801 (2014).